

PLANCK CLUSTER PAPER

SB¹, JPH¹, FM², PD¹

Draft Version July 16, 2018

ABSTRACT

Copied and pasted from proposals. We propose to continue our program of optical imaging to unveil all of the most massive clusters in the observable Universe. We start from the all-sky *Planck* Sunyaev-Zeldovich (SZ) catalogs, which contain several hundred high significance (signal-to-noise ratio, SNR > 5) unconfirmed cluster candidates. Since SZ selection favors high mass clusters and the *Planck* confirmation process favored low redshift systems, the highest significance unconfirmed candidates are, therefore, likely massive clusters ($M_{500} > 5 \times 10^{14} M_\odot$) at relatively high redshift ($z > 0.5$). Our proposed observations, using MOSAIC-3 on Mayall, are designed to confirm the presence of a brightest cluster galaxy (to $z \sim 1$) and red sequence of accompanying cluster members (to $z \sim 0.7$). Preliminary results from our observations over the past two years have validated our approach by the detection of optical clusters in a number of *Planck* candidates, including the discovery of rich systems at $z = 0.553$ and $z = 0.830$ that rival the most massive clusters known. The proposed observations represent the first step required to provide a complete all-sky census throughout the observable Universe of the most massive, high redshift clusters. Their expected high redshift and high mass make the unconfirmed *Planck* clusters, arguably, the most important available sample for probing deviations from Λ CDM and defining the high-mass end of the cluster mass function.

1. INTRODUCTION

this section has not been edited and is just a bunch of stuff copy and pasted. I did update some of the references.

Massive clusters of galaxies are the extraordinary objects which hold important clues to the evolution of structure in the universe. The widely accepted Λ CDM model of cosmology makes specific predictions about the mass distribution of galaxy clusters in the universe. The number of galaxy clusters, especially at high redshifts, can help constrain structure formation models (e.g., Mortonson et al. 2011; Harrison & Coles 2012; Harrison & Hotchkiss 2012; Waizmann et al. 2012; Zitrin et al. 2009). Galaxy clusters also harbor a significant fraction of the visible baryons in the Universe, in the form of a hot intracluster medium that leaves an imprint on the Cosmic Microwave Background (CMB) through the Sunyaev-Zel'dovich effect (SZ; Sunyaev & Zeldovich 1972 effect).

Using the SZ effect to discover clusters of galaxies has the distinct advantage that the surface brightness of the SZ effect does not dim with increasing redshift. This allows homogeneous samples of massive clusters to be detected out to arbitrary distances. Ground based, large area-sky surveys such as those with the Atacama Cosmology Telescope (ACT; Swetz et al. 2011) and the South Pole Telescope (SPT; Carlstrom et al. 2011) have produced catalogs of hundreds of massive clusters below $z \sim 1.4$ (e.g., Hasselfield et al. 2013; ?). Now, *Planck* (Tauber et al. 2010; Planck Collaboration et al. 2011) has released an all-sky SZ sample (PSZ; Planck Collaboration et al. 2014b, 2015) that contains 861 confirmed clusters (of which most [683] were known previously) and another 366 unconfirmed cluster candidates.

Clusters were initially confirmed by cross correlating with previous catalogs (see Section 4; Planck Collabo-

ration et al. 2014b). More recently, dedicated follow up of still-unconfirmed clusters has begun in earnest (e.g., Liu et al. 2015; Planck Collaboration et al. 2015, 2016b; Burenin 2017; Barrena et al. 2018; Amodeo et al. 2018; Streibyanska et al. 2018).

This paper is organized as follows: sections 2 through 4 describe the design, observations, data reduction and calibration, and creation of derived data products. In Section 5, we present the main results of our observations, and discuss the results in Section 6. In Section 7, we summarize the key results and conclude.

Unless otherwise noted, throughout this paper, we use a concordance cosmological model ($\Omega_\Lambda = 0.7$, $\Omega_m = 0.3$, and $H_0 = 70 \text{ km s}^{-1}\text{Mpc}^{-1}$), assume a Chabrier initial mass function (Chabrier 2003), and use AB magnitudes (Oke 1974).

2. DESIGN

Our observational design is motivated by the release of the second, all-sky PSZ catalog³ (hereafter PSZ2; Planck Collaboration et al. 2015) which contains 559 unconfirmed SZ detections with $S/N > 4.5$. We posit that the vast majority of these must lie at $z > 0.4$ because the *Planck* confirmation process (Planck Collaboration et al. 2014b) mostly relied on existing catalogs which have a preference for low- z clusters. Furthermore, the confirmed sample of PSZ2 has only a small fraction (3%) of $z > 0.6$ clusters compared to that expected ($\sim 20\%$) based on the theoretical halo mass function (e.g., Jenkins et al. 2001; Tinker et al. 2008) for mass limit of XXXX (need to get this number). If other clusters as massive like el “El Gordo” exist, they are hiding as high-significance candidates within the objects in this *all-sky* catalog.

The core of our observational design relies on the use of

¹ Rutgers;boada@physics.rutgers.edu

² Illinois

³ http://szcluster-db.ias.u-psud.fr/sitools/client-user/SZCLUSTER_DATABASE/project-index.html

optical imaging to confirm the SZ detections as real clusters and provide photometric redshifts using the multi-color information. This design is based on the previous success with the ACT cluster confirmation process using 4-m class telescopes. For example, assuming WMAP7 cosmology (Komatsu et al. 2011) with the Tinker et al. (2008) halo mass function, there should be only ~ 4 clusters as massive as El Gordo ($\leq 2 \times 10^{15} M_{\odot}$) at $z > 0.6$ in the full area covered by the *Planck* PSZ catalog (83.7% of the sky). Although *Planck*s larger beam size (compared to both ACT and SPT) makes it more sensitive to clusters at lower redshifts (due to their larger projected area on the sky), among the confirmed clusters in the recently released all-sky *Planck* SZ catalog are the two highest significance high-redshift SZ detections from ACT (as well as several other ACT and SPT clusters).

Our strategy for this project is to use the Kitt Peak National Observatory (KPNO) Mayall-4m telescope imaging as the first and fundamental step to confirm the highest significance detections in the PSZ2 catalog that are visible across the entire northern sky. Following closely the procedure used for ACT follow-up (e.g., Menanteau et al. 2013), targets are prioritized by SZ signal-to-noise ratio (SNR). We choose to initially report on targets with PSZ2 SNR > 5 as the statistical reliability of PSZ2 cluster candidates should be quite high: according to the *Planck* team $\sim 90\%$ of candidates at SNR > 5 are expected be “real” clusters (see Figure 11; Planck Collaboration et al. 2016a). Optical imaging should be sufficient to confirm nearly all of the candidates, but for the highest redshift ones, near-IR data will be necessary. Again following the procedure for ACT cluster follow-up: those candidates with some evidence for a high- z brightest cluster galaxy (BCG) will be targeted with near-IR observations to confirm the presence of a BCG and detect the red sequence of cluster members. Observational priority again is given to higher S/N candidates.

2.1. Observations

All observations were conducted with the KPNO Mayall telescope. The optical observations were made with the MOSAIC camera mounted at the prime focus. Two detector packages were used for the observations. The earlier MOSAIC1.1 instrument consisted of eight 2048×4096 SiTe CCDs, arranged 2×4 , separated by a ~ 50 pixels gap with a pixel scale of $0''.26$ pixel $^{-1}$. MOSAIC1.1 was replaced with Mosaic3, in mid-2015, and consists of four new $4k \times 4k$, 15 micron pixel, 500-micron thick LBNL deep-depletion CCDs. Because the only change from MOSAIC1.1 to MOSAIC3 are the CCDs and controllers both versions have a $36' \times 36'$ field-of-view.

The optical observing strategy consists of targeted *griz* observations of individual candidates with total exposure times of 360 s, 360 s, 1100 s and 1100 s (assuming dark conditions). The final exposures consist of four dithered positions with individual exposures of 90 s for the *gr*-bands or 275 s for the *iz*-bands. These exposure times are designed to provide 5σ detections limits of $g = ??$, $r = 24.5$, $i = 24.5$, $z = 24.2$ ensuring the unambiguous detection of the faint (i.e., $0.4L\star$) galaxies in the red cluster sequence up to $z \sim 1.0$ (citation?) and of brightest cluster galaxies (BCGs) to higher redshifts. The choice of filters in our program is driven by the need to segregate early-type galaxies in the cluster through their colors (or

photometric redshifts) by sampling blue-ward and red-ward of the 4000Å break. Our depths are quite a bit different than the designed depths. Should we mention that here, or wait till later on when we are discussing how we actually did?

3. DATA REDUCTION AND CALIBRATION

Standard image reductions including subtraction of dark frames, flat fielding, sky-subtraction, and bad pixel masking was performed by the NOAO virtual observatory using the MOSAIC (Valdes & Swaters 2007) science pipelines. The resultant FITS files consist of fully reduced images with either all single exposure CCDs mosaicked into a single image extension (as in the case of Mosaic1.1) or as a multi-extension FITS file with each single exposure CCD occupying a separate extension.

We then mosaic each separate exposure into a master mosaic as described in the following section.

3.1. Mosaicking

Combined mosaics are created with SWARP (Bertin et al. 2002). We create three distinct types of mosaics. The individual dither frames are stacked and then median combined to produce the final completed science mosaic. A “detection” is created by combining select science mosaics into a “chi2” image using either the *i*- and *z*-band when both are available and of sufficient quality. Finally we create a set of mosaics use to produce the three color image used for cluster finding. We median combine the *griz* science mosaics into a “blue” (*g*-band), “green” (*r*-band), and “red” (*iz*-band) mosaic. All final mosaics have a pixelscale of $0''.25$ /pix. The final exposure time is calculated as the median exposure time of the combined images, and similarly the final airmass is median of the individual air masses. need to talk about the weight images

The full parameter file used while creating the mosaics is given in Appendix ??.

3.2. Astrometric Calibration

Each of the final science mosaics produced in the previous section are first astrometrically aligned with *Gaia* (Gaia Collaboration et al. 2016a) Data Release 1 (Gaia Collaboration et al. 2016b) using SCAMP (Bertin 2006) as a part of PHOTOMETRYPipeline⁴ (PP; Mommert & M. 2017).

Sources are extracted from the mosaics with a signal-to-noise ratio (SNR) of at least ten and with a minimum area of at least 12 pixels. The extracted sources are then matched to the *Gaia* data and a new astrometric solution is calculated. Because the initial astrometric solution from the VO is quite accurate, the resultant corrections are much less than $1''$.

3.3. Photometric Calibration

After the mosaics have been astrometrically aligned, we use PP to produce a photometric solution. PP calculates a photometric zero-point in each of our observed bands by comparing field stars located throughout the mosaic to known photometry from large-area sky surveys. Because our sources are spread across the entire northern sky, and because we prefer to minimize

⁴ <https://github.com/mommert/photometrystreamline>

the number of differences between photometric solutions we are limited to two optical surveys. For the optical data, we first seek photometric data from the *Sloan Digital Sky Survey* (SDSS; York et al. 2000) Data Release 13 (DR13; Albareti et al. 2017). When our target does not lie within the SDSS footprint we utilize the Panoramic Survey Telescope and Rapid Response System (Pan-STARRS; Chambers et al. 2016) Data Release 1 (hereafter PS1; Flewelling et al. 2016). Both surveys provide accurate *griz* magnitudes and large on-line queryable databases for rapid automated calibration.

Sources are extracted from the combined mosaics with either a 3'' or 8'' diameter aperture for optical sources respectively; sources with a SNR ≥ 10 are matched to a survey catalog and a photometric zero-point is determined. We use half of the available stars (with accurate catalog photometry) to derive the zero-point resulting in zero-points calculated from approximately 10 – 500 stars and with typical uncertainties of 0.05 mag for the *griz*-bands and 0.16 mag for the *z*-band.

Should we talk about the difference between us and SDSS? If so, how should we “sum up” the differences in a simple way?

4. ANALYSIS

Lorem ipsum dolor amet swag copper mug meh tilde, put a bird on it live-edge tattooed kinfolk before they sold out locavore selvage leggings raclette literally bicycle rights. Hot chicken kickstarter mustache vinyl roof party. Wayfarers brooklyn truffaut twee umami, venmo irony. Typewriter viral pop-up, listicle vaporware organic af salvia keytar twee chillwave austin +1 offal blog. La croix dreamcatcher snackwave, try-hard intelligentsia taxidermy messenger bag air plant godard mustache celiac glossier echo park. Photo booth readymade authentic glossier biodiesel snackwave beard hammock sriracha before they sold out edison bulb fixie PBR&B. Man bun pabst kogi, crucifix subway tile af tacos cray tumeric lyft cronut lomo tattooed.

4.1. Source Extraction and Photometry

For source extraction and photometry estimation we use Source Extractor (hereafter SExtractor; version 2.19.5; Bertin & Arnouts 1996) run dual image mode with the CHI2 detection image as the detection image. See Section 3.1. See Appendix ?? for a complete parameter listing.

4.2. Photometric Redshifts

We determine photometric redshifts ($\text{photo-}z$) from the five-band optical images using Bayesian Photometric Redshifts (BPZ; Benitez 2000; Coe et al. 2006) following the same procedure as in Menanteau et al. (2009).

We assess the effectiveness of our $\text{photo-}z$ estimates by comparing with the available spectroscopic redshifts ($\text{spec-}z$) from the SDSS. We use three diagnostics to gauge $\text{photo-}z$ accuracy. First, we report the full scatter between the $\text{photo-}z$ and $\text{spec-}z$, defined as:

$$\sigma_f = \text{RMS}[\delta z / (1 + z_{\text{spec}})] \quad (1)$$

where $\delta z = z_{\text{spec}} - z_{\text{phot}}$. Second, we report the normalized median absolute deviation (NMAD; Ilbert et al.

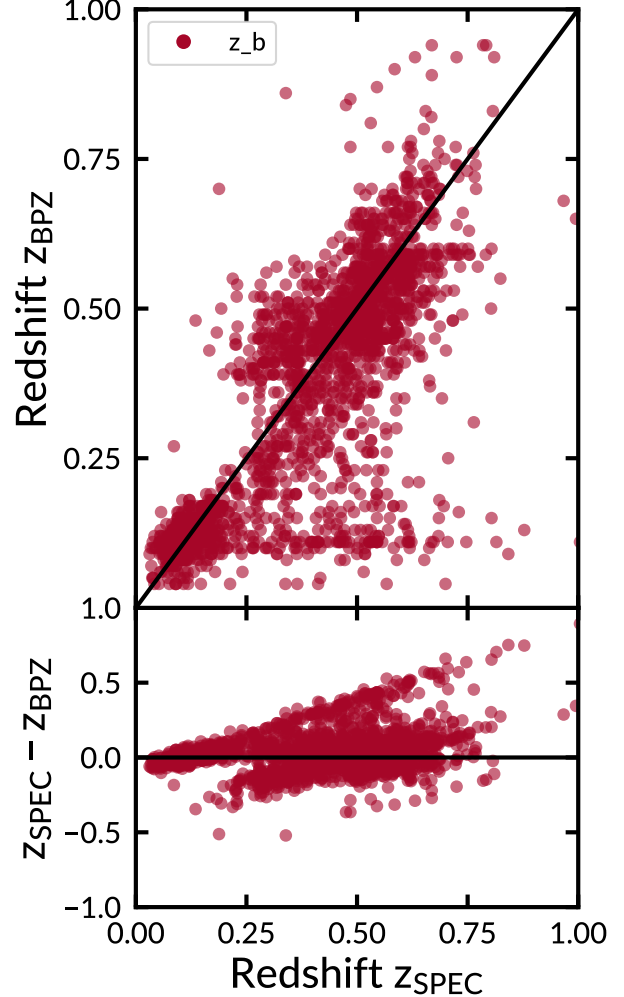


FIG. 1.— Comparison between photometric and spectroscopic redshifts for 2253 galaxies which have spectroscopic redshifts from the SDSS. The photometric redshifts in the top panel use a Bayesian approach with a custom empirical prior on galaxy brightness for the photometric redshifts. The bottom panel shows the difference between the spectroscopic and photometric redshift.

2009; Dahlen et al. 2013; Molino et al. 2017), given as

$$\sigma_{\text{NMAD}} = 1.48 \times \text{median}\left(\frac{|\delta z|}{1 + z_{\text{spec}}}\right). \quad (2)$$

which provides an estimate of the scatter resistant to catastrophic outliers. Finally, the catastrophic outlier fraction (OLF) where we define a catastrophic outlier (following Molino et al. 2017) as,

$$\eta = \frac{|\delta z|}{(1 + z_{\text{spec}})} > 5 \times \sigma_{\text{NMAD}}. \quad (3)$$

Figure 1 shows the photometric redshift performance as a function of the true spectroscopic redshift. For the full sample of galaxies we calculate $\sigma_f = \text{XX}\%$, $\sigma_{\text{NMAD}} = \text{XX}\%$, and an outlier fraction, $\eta = \text{XX}\%$. When considering the performance of only the galaxies BPZ classified as E and E/S0 type, we find the following results; $\sigma_f = 10.4\%$, $\sigma_{\text{NMAD}} = 5.43\%$, and an outlier fraction, $\eta = 2.97\%$.

4.3. Cluster Finding

In this section, we briefly describe the algorithms and methods used to select the galaxy clusters from the multi-wavelength optical imaging. We follow the methods described in detail in Menanteau et al. (2009, 2010a). We direct the reader there for an in depth description and discussion of the methods.

We first create a three-color image using STIFF (Bertin & Emmanuel 2011). The red, green, and blue channels are given by the corresponding combined mosaics described in Section 3.1. We then visually inspect an area of roughly $8' \times 8'$ centered on the position of each unconfirmed cluster. Potential brightest cluster galaxies (BCGs) are identified by first calculating the absolute limiting magnitude **needs details**.

Once a potential BCG is selected, the algorithm selects nearby galaxies, within $|z_{BCG} - z| < 0.05$ and 0.5 Mpc projected radius, which BPZ has classified as either E or E/S0 galaxies. These photo-z's of the galaxies are combined using a 3σ median sigma-clipping algorithm to estimate the cluster's mean redshift, z_c . We use this mean cluster redshift measurement and the member selection criteria given previously to estimate the number of cluster members within 1 Mpc, $N_{1\text{Mpc}}$, which we define as the richness of the cluster, N_{gal} .

We correct the N_{gal} estimate by subtracting a statistical background of galaxies. We first estimate the number of background ellipticals by selecting galaxies within an annulus ($R_{200} < r < 2R_{200}$) around each cluster's position. We include galaxies with $\delta z = 0.05$ and similar colors as those galaxies assumed to belong to the cluster. These galaxies are subtracted from the cluster's population which provides an corrected N_{gal} , N_{galc} , which we then use to compute other important quantities. In practice the corrected number of galaxies is between 15% and 20% lower than the uncorrected number (Menanteau et al. 2010a). We report N_{galc} for the remainder of this work.

4.4. Recovery of the Brightest Cluster Galaxies

We have designed our observations to detect BCGs to $z \sim 1.5$. To quantify the actual depth of our images, we perform a Monte Carlo simulation by injecting artificial sources and computing their recovery fraction. We create the artificial sources with the MODELING package, part of ASTROPY (The Astropy Collaboration et al. 2013).

Following the procedure given in Menanteau et al. (2010b), the synthetic galaxies are created to have de Vaucouleurs (de Vaucouleurs 1948) profiles and surface brightnesses corresponding to their magnitude and assumed sizes. We inject the artificial galaxies into our science images with similar noise characteristics as their real counterparts.

We generate four rounds of one hundred elliptical galaxies spread randomly across our science imaging. Each round of galaxies are placed at different random positions to suppress abnormally boosted recovery fractions due to source confusion. The artificial galaxies have total fluxes corresponding to apparent magnitudes between 19 mag $< i < 27$ mag with 0.1 mag spacing.

This is almost directly taken from FM2010 – edit. We use the individual field's completion limit to estimate the redshift to which we can reliably detect massive clus-

ters. For this, we compare the completeness limits of our observations to the expected and observed (i.e., known) apparent magnitudes of galaxies in clusters as a function of redshift. We estimated the expected apparent galaxy i -band magnitude as a function of redshift using L_* as defined for the population of red galaxies by Blanton et al. (2003) at $z = 0.1$ and allowing passive evolution according to a solar metallicity (Bruzual & Charlot 2003) $\tau = 1.0$ Gyr burst model formed at $zf = 5$. We show this in Figure 2 for a range of luminosities (L_* , $0.4L_*$, and $4L_*$) aimed at representing the cluster members from the faint ones to the BCG.

5. RESULTS

In this section, we give the results of our cluster finding. We report high confidence, high richness clusters. A high confidence result consists of a clear BCG and many accompanying satellite galaxies. For the 85 fields observed with MOSAIC, we observe fifteen high confidence clusters (see Figures 3–6). In the following subsections we present on each of the eight high confidence observations individually, and group the medium and low confidence observations together.

5.1. Notes on Specific Clusters

In the following subsections, we note previously known sources by querying the NASA/IPAC Extragalactic Database (NED)⁵ and the SIMBAD (Set of Identifications, Measurements, and Bibliography for Astronomical Data) astronomical database⁶ (Wenger et al. 2000). We include sources from the NRAO (National Radio Astronomy Observatory) VLA (Very Large Array) Sky Survey (NVSS; Condon et al. 1998), the Röntgensatellit (ROSAT) All-Sky Survey Bright Source Catalog (RASS-BSC; Voges et al. 1999), the ROSAT All-Sky Faint Source Catalog (RASS-FSC; Voges et al. 2000), and the SDSS. We make note of x-ray and radio sources within $5'$ of the reported BCG pointing and other catalogs as pertinent to the individual cluster.

5.1.1. PSZ1 G084.62-15.86

We recover a cluster at $z_{cl} = 0.27 \pm 0.09$ with 18 members. This is a system with at least three possible BCGs. From the chosen BCG, there are two faint RASS-FSC sources $0'36$ and $0'84$ away from the reported BCG coordinate. Also, there are two NVSS sources $0'66$ and $2'82$ from the BCG pointing with log flux densities of 1.29 and 0.48 mJy at 1.4 GHz. This cluster, with a PSZ1 ID of 283, has been previously confirmed by the *Planck* team; where they found the photometric redshift of the cluster at $z_{spec} = 0.364 \pm \text{none}$ (Planck Collaboration et al. 2016b).

5.1.2. PSZ1 G206.45+13.89

We find a cluster at $z_{cl} = 0.39 \pm 0.05$. We detect 73 potential cluster members, although a bright star ($V = 4.5$ mag; Høg et al. 2000) only $\sim 4'9$ away from the reported BCG. The contaminating star prevents an accurate photo-z estimate for many cluster cluster members. This system has four NVSS sources $0'63$, $2'86$, $4'08$, and

⁵ <https://ned.ipac.caltech.edu/>

⁶ <http://simbad.u-strasbg.fr/simbad/>

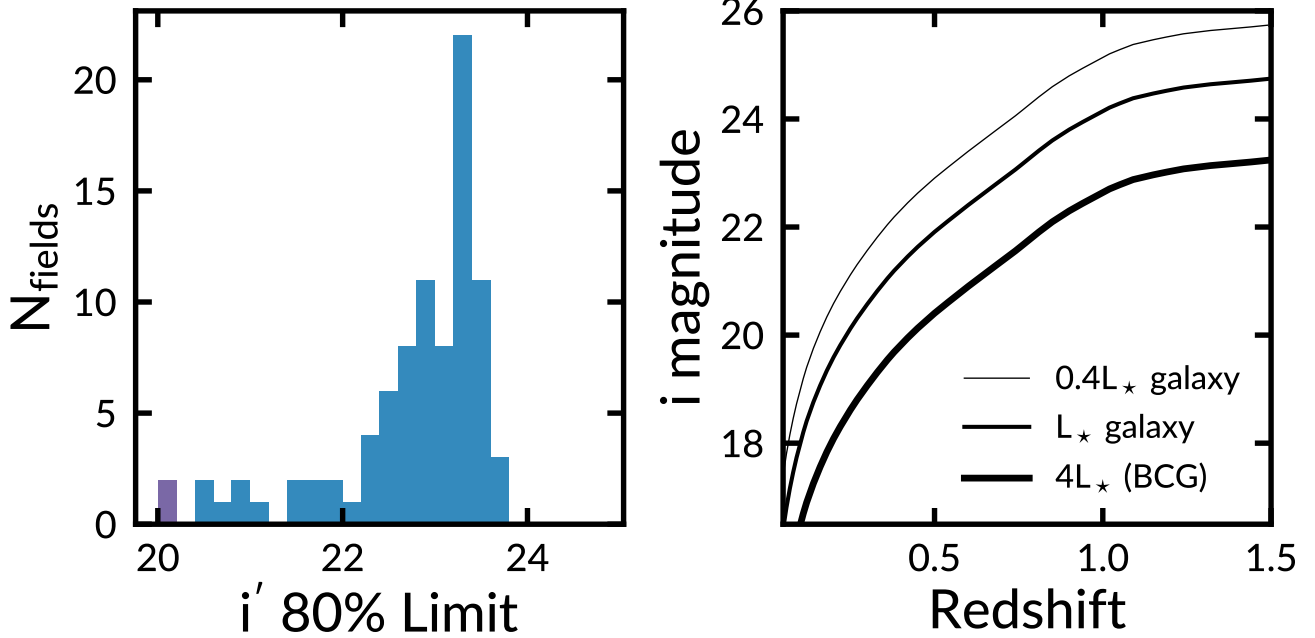


FIG. 2.— *Left:* Histogram of the i' -band magnitude corresponding to 80% completeness in galaxy recovery. When 80% completeness is not achieved we show the limiting magnitude with the highest completeness. *Right:* Observed i' -band magnitudes of L_* , $0.4L_*$, and $4L_*$ (BCG) early-type galaxies as a function of redshift. We define an LL_* galaxy following Blanton et al. (2003) as a population of red galaxies at $z = 0.1$ and allow it to evolve passively. The left and right panels can be combined to estimate the limiting redshift to which we could identify galaxy clusters.

TABLE 1

SUMMARY OF CLUSTER FINDING: COLUMN 1: THE PSZ CLUSTER NAME; COLUMN 2: PSZ2 SNR; COLUMN 3: BCG RIGHT ASCENSION IN J2000; COLUMN 4: BCG DECLINATION IN J2000; COLUMN 5: BCG SEPARATION FROM PSZ POSITION IN ARCMINTUES; COLUMNS 6: CLUSTER REDSHIFT; COLUMN 7: CLUSTER REDSHIFT UNCERTANTY; COLUMN 8: CORRECTED NUMBER OF MEMBER GALAXIES; COLUMN 9: NEW DISCOVERY?

Cluster (1)	SNR (2)	α (J2000) (3)	δ (J2000) (4)	Sep. ('') (5)	z_{cl} (6)	z_{clerr} (7)	N_{gal_c} (8)	New (9)
PSZ1 G084.62 – 15.86	6.01	21 : 49 : 42.524	+33 : 09 : 17.29	1.14	0.27	0.10	18	
PSZ1 G206.45 + 13.89	5.90	07 : 29 : 51.234	+11 : 56 : 31.31	1.97	0.40	0.05	73	
PSZ1 G224.82 + 13.62	5.51	08 : 01 : 41.492	-04 : 03 : 44.48	0.17	0.24	0.04	38	
PSZ2 G029.66 – 47.63	5.74	21 : 45 : 29.940	-21 : 43 : 26.29	4.73	0.34	0.03	130	✓
PSZ2 G043.44 – 41.27	5.55	21 : 36 : 43.728	-10 : 19 : 02.15	1.24	0.42	0.04	116	✓
PSZ2 G096.43 – 20.89	5.81	22 : 48 : 09.402	+35 : 33 : 49.45	0.49	0.24	0.04	54	✓
PSZ2 G098.38 + 77.22	5.51	13 : 18 : 08.274	+38 : 30 : 20.10	5.84	0.78	0.05	58	✓
PSZ2 G106.11 + 24.11	5.70	19 : 21 : 31.852	+74 : 33 : 27.17	0.51	0.14	0.06	0	✓
PSZ2 G107.83 – 45.45	7.09	00 : 07 : 35.605	+16 : 07 : 02.39	0.83	0.54	0.05	30	✓
PSZ2 G120.76 + 44.14	5.59	13 : 12 : 53.537	+72 : 55 : 06.05	2.02	0.35	0.03	92	✓
PSZ2 G125.55 + 32.72	6.49	11 : 25 : 34.008	+83 : 58 : 55.75	1.44	0.21	0.06	32	✓
PSZ2 G137.24 + 53.93	7.87	11 : 40 : 59.525	+61 : 07 : 07.07	4.61	0.45	0.06	40	✓
PSZ2 G173.76 + 22.92	5.80	07 : 17 : 26.636	+44 : 05 : 02.97	1.62	0.14	0.04	0	✓
PSZ2 G191.82 – 26.64	6.17	04 : 38 : 28.283	+04 : 37 : 19.91	5.18	0.18	0.06	24	✓
PSZ2 G305.76 + 44.79	5.72	12 : 59 : 53.612	-18 : 01 : 35.05	0.44	0.74	0.08	48	✓

4'.60 away from the BCG pointing. They possess a log flux density of 1.12, 0.7, 0.46, and 1.65 mJy respectively at 1.4 GHz. This cluster has been previously confirmed in (Barrena et al. 2018) as a rich, massive cluster. It has been recognized with the PSZ1 ID 682 where they found a photometric redshift of $z_{phot} = 0.44 \pm 0.04$.

5.1.3. PSZ1 G224.82+13.62

This system, at $z_{cl} = 0.23 \pm 0.05$ has two NVSS sources 2'.09 and 4'.10 away from the *Planck* pointing. The sources possess a log flux density of 0.51 and 0.86 mJy respectively at 1.4 GHz. According to the SIMBAD search

there is an Einstein Observatory soft x-ray source 0'.316 away from the BCG pointing (2). This cluster has also been confirmed in the (Barrena et al. 2018) as a rich, massive cluster with the PSZ1 ID 752 and a photometric redshift of $z_{cl} = 0.25 \pm 0.03$.

5.1.4. PSZ2 G029.66-47.63

Check the citations for the two RASS sources. Did they come from the same place or are they a bright and a faint source? SIMBAD has no reference for the position instead it points the external catalog VizieR, it displays the bright and faint ROSAT catalogs but there

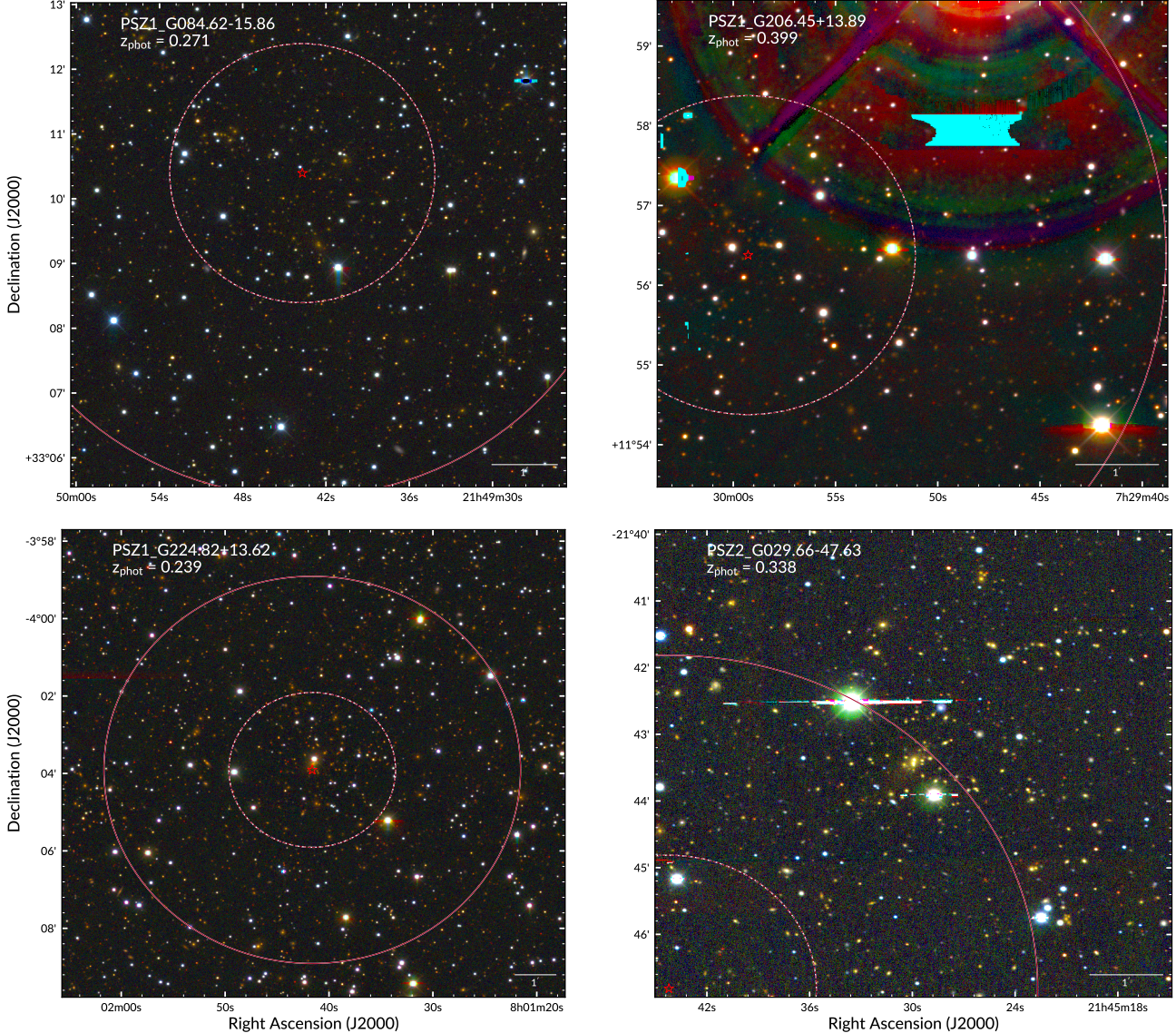


FIG. 3.— RGB (*irg*) color images for four PSZ clusters optically confirmed using the our optical imaging. Each panel is centered on the cluster’s BCG and has a width of 1 mpc at the corresponding cluster’s redshift. The horizontal bar in the lower left of each panel shows the scale of the panel, where north is up and east is to the left. The location of the PSZ detection is denoted by a red star. The dashed and solid concentric circles are 2' and 5' in radius respectively.

is no information in the bright catalog. Following the faint catalog the first author is Voges. The PSZ2 cluster at $z_{cl} = 0.33 \pm 0.03$ has one NVSS source 3.20'' away from the BCG coordinate with a log flux density of 0.8 mJy at 1.4 GHz, and one RASS-FSC 0.34'' away from the reported BCG pointing. From the SIMBAD search there is a ROSAT faint x-ray source 2.84'' away from the BCG coordinates (Bohringer et al. 2000).

5.1.5. PSZ2 G043.44-41.27

We find this system at $z_{cl} = 0.41 \pm 0.03$ with one NVSS source 1.37'' away from the BCG coordinate. The radio source is a symmetric double with a log flux density of 2.71 mJy at 0.365 GHz. Also, from the SIMBAD search there is a RASS-FSC 0.16'' away from the cluster BCG (Bohringer et al. 2000).

5.1.6. PSZ2 G096.43-20.89

At $z_{cl} = 0.24 \pm 0.03$ this system has one RASS-BSC source 1.44'' away from the BCG position. There are three NVSS sources 4.18'', 4.86'', and 4.89'' from the BCG position. The log flux densities are 1.46, 0.72, and 1.39 mJy respectively at 1.4 GHz. There is a Zwicky cluster 3.55'' away from the BCG position that is 17'' in diameter with a richness of 89. It is classified as medium compact (Zwicky & Kowal 1968).

5.1.7. PSZ2 G098.38+77.22

This cluster at $z_{cl} = 0.77 \pm 0.05$ has a Faint Images of the Radio Sky at Twenty-centimeters (FIRST; Becker et al. 1995) source 1.76'' from the BCG position with a log flux density of 0.10 mJy at 1.4 GHz. There is a SDSS galaxy that is 1.44'' away with a spectral redshift of 0.726. Cite individual SDSS DR?. And a quasi stellar object 2.02'' away from the BCG position with a redshift of 0.2 (85).

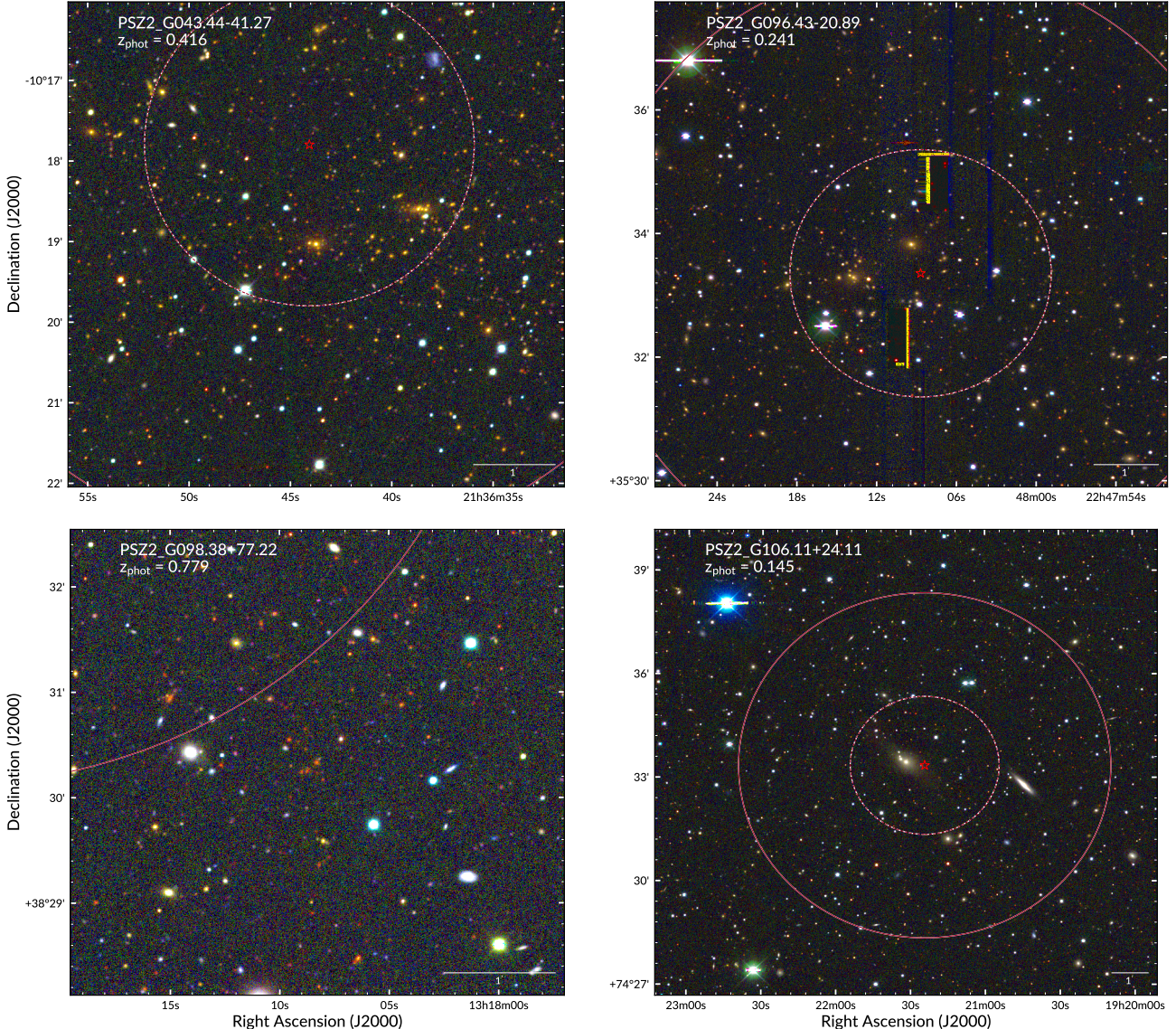


FIG. 4.— RGB (*irg*) color images for four PSZ clusters optically confirmed using the our optical imaging. Each panel is centered on the cluster’s BCG and has a width of 1 mpc at the corresponding cluster’s redshift. The horizontal bar in the lower left of each panel shows the scale of the panel, where north is up and east is to the left. The location of the PSZ detection is denoted by a red star. The dashed and solid concentric circles are 2' and 5' in radius respectively.

5.1.8. PSZ2 G106.11+24.11

NED gives a broken ads link but it does give the title, when I search on title instead of the WGA I’m lead to the citation We find this system at $z_{cl} = 0.14 \pm 0.06$ with a RASS-BSC source and a WGA ROSAT source 0'26 and 0'21 away from the BCG position respectively. [check peter’s vizier catalog citation](#). According to the SIMBAD search, there is a RASS x-ray cluster 0'84 away from the BCG pointing (Bohringer et al. 2000). [The citation from SIMBAD is given directly with the ICRS coordinates, not form external catalog](#). And the first author on this is Bohringer

5.1.9. PSZ2 G107.83-45.45

This cluster at $z_{cl} = 0.54 \pm 0.05$ has a NVSS source 1'28 from the BCG postion with a log flux density of 0.89 mJy at 1.4 GHz, and a SDSS galaxy 1'89 away with

a spectral redshift of 0.566 (61).

5.1.10. PSZ2 G120.76+44.14

At an estimated $z_{cl} = 0.34 \pm 0.03$, this cluster has an ABELL HHP90 galaxy 0'11 away with a spectral redshift of 0.29 (Huchra et al. 1990), and a RASS-FSC source 0'17 from the BCG pointing (Voges et al. 2000). From the SIMBAD search there is an Einstein extended x-ray source 1'67 away from the BCG pointing (Oppenheimer et al. 1997), and a Zwicky cluster 2'67 away (6).

5.1.11. PSZ2 G125.55+32.72

We estimate this PSZ2 source at $z_{cl} = 0.21 \pm 0.06$. It has a Westerbork Northern Sky Survey (WENSS) radio source 0'17 away with a log flux density of 1.61 mJy at 0.325 GHz (Rengelink et al. 1997). There is also a NVSS source 2'92 away at 1.62 mJy at 0.325 GHz, and a bright

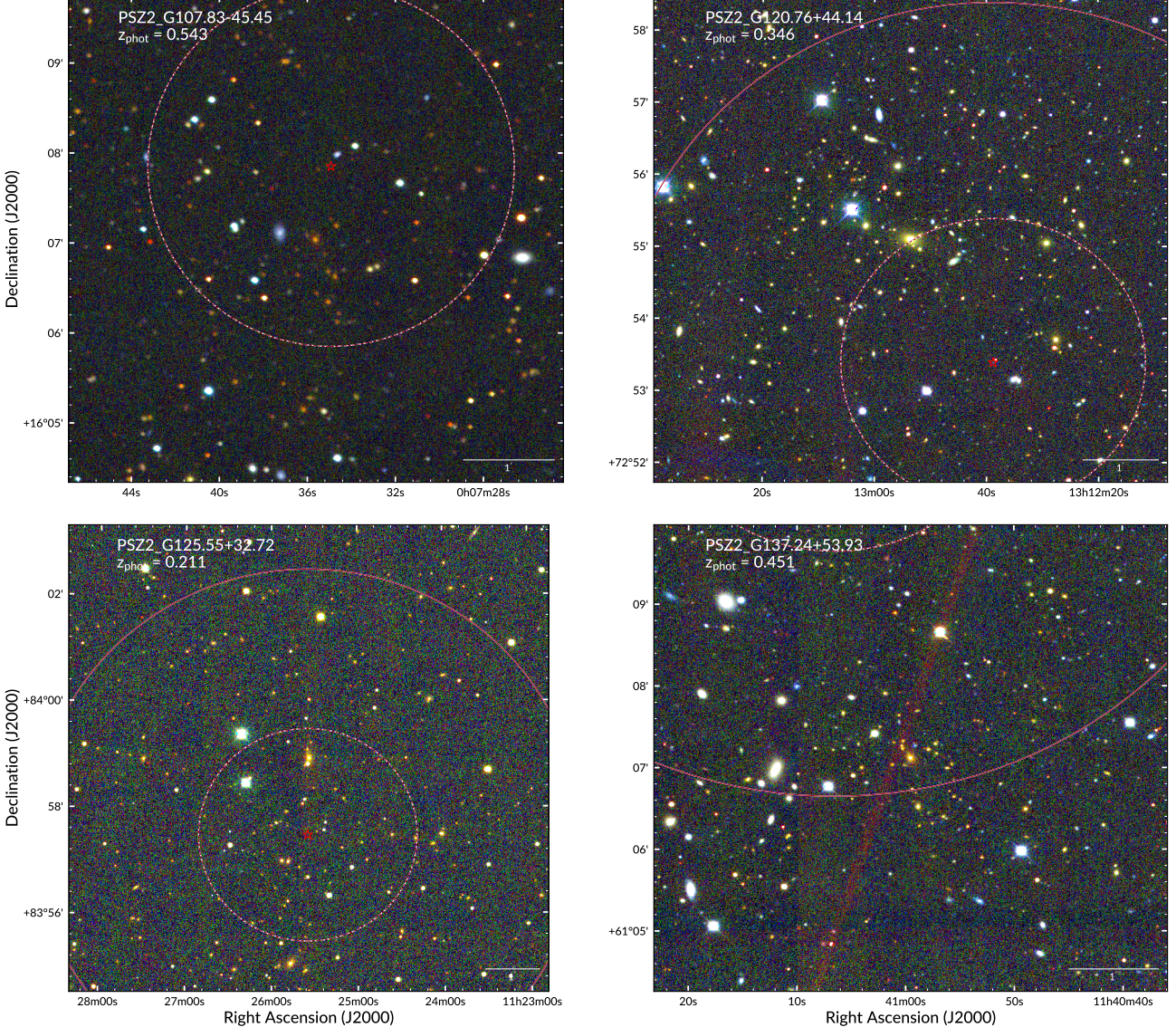


FIG. 5.— RGB (*irg*) color images for four PSZ clusters optically confirmed using the our optical imaging. Each panel is centered on the cluster’s BCG and has a width of 1 mpc at the corresponding cluster’s redshift. The horizontal bar in the lower left of each panel shows the scale of the panel, where north is up and east is to the left. The location of the PSZ detection is denoted by a red star. The dashed and solid concentric circles are 2' and 5' in radius respectively.

RASS-BSC 2.96 away from the BCG pointing. A littler farther out there are two more NVSS sources 3.81 and 4.98 away, at 0.56 and 1.02 mJy respectively at 1.4 GHz.

5.1.12. PSZ2 G137.24+53.93

This cluster at $z_{cl} = 0.45 \pm 0.05$, has a NVSS source 0.14 away from the BCG pointing with a log flux density of 1.46 mJy at 1.4 GHz. Also a VFK2015 radio source 0.27 away (2), and two radio sources, a Sixth Cambridge, and NVSS source at 0.715, and 3.826 away respectively. The Sixth Cambridge and the NVSS sources have log flux densities of 3.09 and 0.94 mJy at 0.151 and 1.4 GHz (6,40).

5.1.13. PSZ2 G173.76+22.92

[need help on B3 citation](#) This system at $z_{cl} = 0.13 \pm 0.03$ has a Third Bologna catalog galaxy 0.012 away at a

redshift of 0.06 (Ficarra et al. 1985). It also possesses a VFK2015 radio source 0.16 away from the BCG pointing (2), and two radio sources, a Sixth Cambridge, and NVSS source at 0.715, and 3.826 away respectively. The Sixth Cambridge and the NVSS sources have log flux densities of 3.09 and 0.94 mJy at 0.151 and 1.4 GHz (6,40).

5.1.14. PSZ2 G191.82-26.64

This cluster at $z_{cl} = 0.18 \pm 0.06$ has four NVSS sources 0.981, 2.346, 2.585, and 4.570 away from the BCG coordinate. They possess a log flux density of 0.97, 1.39, 1.36, 1.12 mJy at 1.4 GHz.

5.1.15. PSZ2 G305.76+44.79

Finally, at $z_{cl} = 0.73 \pm 0.07$, this cluster has a PMN radio source 0.019 away from the BCG coordinate with a log flux density of 1.71 mJy at 4.85 GHz (Griffith & Wright 1993).

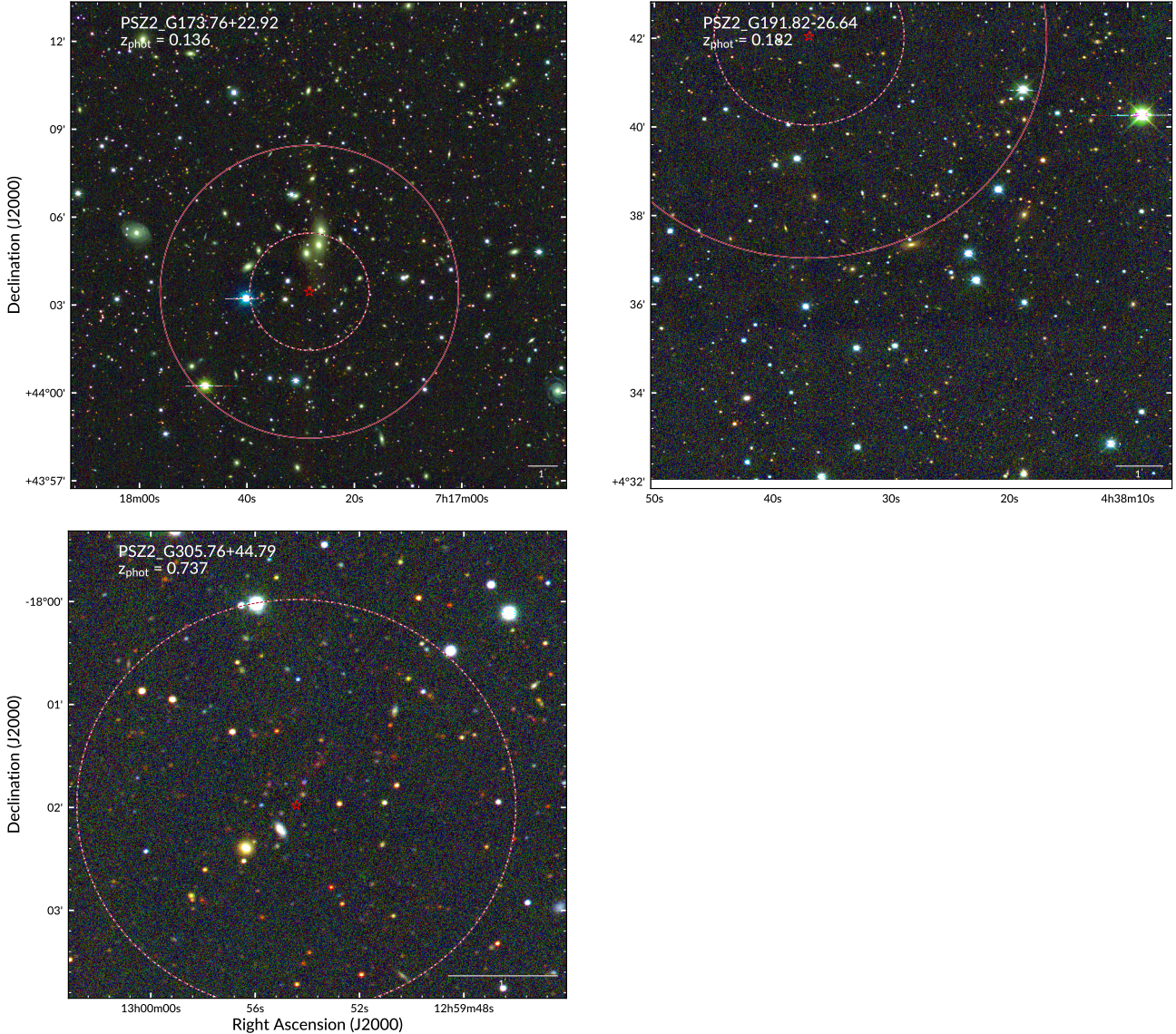


FIG. 6.— RGB (*irg*) color images for four PSZ clusters optically confirmed using the our optical imaging. Each panel is centered on the cluster’s BCG and has a width of 1 mpc at the corresponding cluster’s redshift. The horizontal bar in the lower left of each panel shows the scale of the panel, where north is up and east is to the left. The location of the PSZ detection is denoted by a red star. The dashed and solid concentric circles are 2' and 5' in radius respectively.

6. DISCUSSION

In this section, we discuss the results given in the previous section as a whole, and frame those results in the context of the broader PSZ sample. From the 85 fields observed, we identified fifteen rich cluster systems at $0.1 < z_{cl} < 0.8$. Because our observations are limited to objects with $\text{SNR} > 5\sigma$, we would expect at most one failed detection. This leads to three possible alternatives.

1. The vast majority of clusters in our sample at low- z .
2. The vast majority of the clusters in our sample lie at redshifts beyond our optical detection limits.
3. The vast majority of clusters are obscured by the Milky Way.

4. The vast majority of cluster candidates in our sample are not true 5σ detections.

One: The initial design of our survey uses an $8' \times 8'$ search window centered on the PSZ position. Low- z clusters could appear as isolated elliptical galaxies and thus would not be classified as clusters. In follow up inspection of the full-sized mosaics, approximately 1 degree², reveals no such low- z structures. In addition, we compute the expected fraction of galaxy clusters as a function of redshift from the cluster mass function of Tinker et al. (2008). Figure 7 shows the expected cumulative distributions of three intermediate mass clusters, solid lines, as well as the distribution of confirmed PSZ clusters. The previously confirmed cluster sample includes results from dedicated follow up by the *Planck* team (e.g., Planck Collaboration et al. 2015, 2016b). From these numerical simulations we know that a low fraction (< 5%) of all

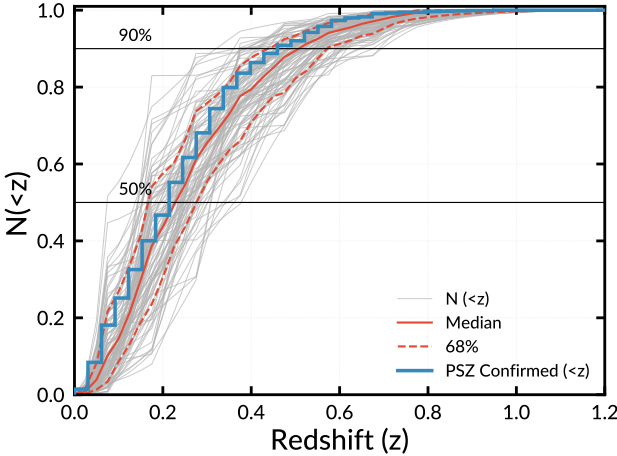


FIG. 7.— The predicted number of clusters more massive than $M_{500c} = 3, 6$ and $9 \times 10^{14} M_\odot$ (solid lines) as a function of redshift and normalized to unity from the mass function of Tinker et al. (2008). For reference we show the 50% and 90% fractional completeness levels. The blue histogram shows the normalized cumulative distribution of confirmed PSZ clusters.

clusters with $M_{500} = 3 - 9 \times 10^{14} M_\odot$ are expected to reside at redshifts less than 0.1. Of the 85 fields observed, we expect approximately four clusters to lie at such low redshifts. We recover three low- z clusters during the course of our analysis.

Two: The median limiting i -band magnitude of our survey is 23 mag, corresponding to a limiting redshift of $z = 0.72$ for an M_* galaxy. While it is possible that a number of cluster candidates corresponding to real clusters exists above this redshift, it is unlikely that these correspond to a population of the high SNR objects targeted by this survey. Massive clusters, such as those targeted by this survey, are exceedingly rare objects. For example there are only twelve clusters at $z > 0.72$ in PSZ2, only five of which are above $z = 0.8$. Again, Figure 7 allows us to estimate the number of clusters missed with our observing limits. At $z > 0.7$, we expect $\sim 18\%$ of clusters with $M_{500c} = 3 \times 10^{14} M_\odot$, corresponding to only fifteen clusters of our 85 observed fields. While high- z objects were expectedly missed by this survey, high- z objects alone cannot account for the high number of still unconfirmed clusters. We expect further follow up observations with deep infrared imaging will be required to place further limits on these high- z objects.

Three: Jack mentioned that we can look at the distributions as a function of galactic latitude. If we are primarily finding galaxies which are far away from the galaxy there may be some argument to be made that there are many clusters hiding behind the stars in the Milky Way.

Four: Perhaps the most plausible explanation is that no optical counterpart to the PSZ detection exists. Previous works (e.g., Barrena et al. 2018) find a similar fraction of non-detections, and consider both high noise values in the $Planck Y_{500}$ maps (Planck Collaboration et al. 2014a) along with contamination from foreground radio sources. As part of our NED search, we find that approximately 75% of confirmed PSZ sources have a NVSS radio source (39.6 mJy average flux) within 5' of the PSZ position. unconfirmed PSZ sources show slightly fewer

sources with approximately 55% having a NVSS radio source (25.1 mJy average flux) within 5'.

5σ corresponds to 99.999426697% purity or 1/1744278 will be false.

7. SUMMARY

following FM2010

In this work, we report on our analysis of seventeen nights of observing spread over three years (2014–2017). We utilize and independently develop a pipeline to process the $griz$ imaging taken with both the MOSAIC 1.1 and MOSAIC 2 imagers on the KPNO Mayall-4m telescope. We present the first results from the complete data set of 85 fields, fifteen rich galaxy clusters of which twelve were previously unknown.

The newly discovered clusters range in photometric redshift between $0.13 < z < 0.74$. The upper redshift limit is due to the depth of imaging restricting us to clusters at $z < 0.8$. This prevents us from finding the most interesting rich clusters at very high redshifts.

A large motivation for this work has come from the recent successes of other SZ follow up programs (e.g., Bayliss et al. 2016; Sifón et al. 2016; Kirk et al. 2015). We present this sample of clusters to aid in the confirmation of the PSZ sources, and to potentially reveal clusters with interesting astrophysical properties. The PSZ sources which remain unconfirmed have the potential to be the most interesting.

In future work, we will present the properties of lower richness clusters and small groups of galaxies in addition to multi-wavelength studies using the clusters detected as part of this survey.

ACKNOWLEDGEMENTS

This work was supported by NASA Astrophysics Data Analysis grant number NNX14AF73G and NSF Astronomy and Astrophysics Research Program award number 1615657. This research made use of several open source packages: APLPY, an open-source plotting package for Python hosted at <http://aplpy.github.com>; the IPYTHON package (Perez & Granger 2007); MATPLOTLIB, a Python library for publication quality graphics (Hunter 2007) and ASTROPY, a community developed core Python package for Astronomy (The Astropy Collaboration et al. 2013). IRAF is distributed by the National Optical Astronomy Observatory, which is operated by the Association of Universities for Research in Astronomy under cooperative agreement with the National Science Foundation (Tody 1993). PYRAF is a product of the Space Telescope Science Institute, which is operated by AURA for NASA. Funding for the SDSS and SDSS-II has been provided by the Alfred P. Sloan Foundation, the Participating Institutions, the National Science Foundation, the U.S. Department of Energy, the National Aeronautics and Space Administration, the Japanese Monbukagakusho, the Max Planck Society, and the Higher Education Funding Council for England. The SDSS Web Site is <http://www.sdss.org/>. The SDSS is managed by the Astrophysical Research Consortium for the Participating Institutions. This work has made use of data from the European Space Agency (ESA) mission *Gaia* (<https://www.cosmos.esa.int/gaia>), processed by the *Gaia* Data Processing and Analysis Consortium (DPAC, <https://www.cosmos.esa.int/web/>

[gaia/dpac/consortium](#)). Funding for the DPAC has been provided by national institutions, in particular the institutions participating in the *Gaia* Multilateral Agreement. This research has made use of the VizieR catalogue access tool, CDS, Strasbourg, France. The original description of the VizieR service was published in Ochsenbein et al. (2000). This research has made use of the SVO Filter Profile Service (<http://svo2.cab.inta-csic.es/theory/fps/>).

supported from the Spanish MINECO through grant AyA2014-55216. This research has made use of the NASA/IPAC Extragalactic Database (NED) which is operated by the Jet Propulsion Laboratory, California Institute of Technology, under contract with the National Aeronautics and Space Administration.

REFERENCES

- Albareti, F. D., Prieto, C. A., Almeida, A., et al. 2017, The Astrophysical Journal Supplement Series, 233, 25
- Amodeo, S., Mei, S., Stanford, S. A., et al. 2018, The Astrophysical Journal, 853, 36
- Barrena, R., Streblyanska, A., Ferragamo, A., et al. 2018, eprint arXiv:1803.05764, arXiv:1803.05764
- Bayliss, M. B., Ruel, J., Stubbs, C. W., et al. 2016, The Astrophysical Journal Supplement Series, 227, 3
- Becker, R. H., White, R. L., & Helfand, D. J. 1995, The Astrophysical Journal, 450, 559
- Benítez, N. 2000, The Astrophysical Journal, 536, 571
- Bertin, E. 2006, in Astronomical Society of the Pacific Conference Series, Vol. 351, Astronomical Data Analysis Software and Systems XV, ed. C. Gabriel, C. Arviset, D. Ponz, & S. Enrique, 112
- Bertin, E., & Arnouts, S. 1996, Astronomy and Astrophysics Supplement Series, 117, 393
- Bertin, E., & Emmanuel. 2011, Astrophysics Source Code Library, record ascl:1110.006
- Bertin, E., Mellier, Y., Radovich, M., et al. 2002, in Astronomical Society of the Pacific Conference Series, Vol. 281, Astronomical Data Analysis Software and Systems XI, ed. D. Bohlender, D. Durand, & T. Handley, 228
- Blanton, M. R., Hogg, D. W., Bahcall, N. A., et al. 2003, The Astrophysical Journal, 592, 819
- Borriinger, H., Voges, W., Huchra, J. P., et al. 2000, The Astrophysical Journal Supplement Series, 129, 435
- Bruzual, G., & Charlot, S. 2003, Monthly Notices of the Royal Astronomical Society, 344, 1000
- Burenin, R. A. 2017, Astronomy Letters, 43, 507
- Carlstrom, J. E., Ade, P. A. R., Aird, K. A., et al. 2011, Publications of the Astronomical Society of the Pacific, 123, 568
- Chabrier, G. 2003, Publications of the Astronomical Society of the Pacific, 115, 763
- Chambers, K. C., Magnier, E. A., Metcalfe, N., et al. 2016, eprint arXiv:1612.05560, arXiv:1612.05560
- Coe, D., Benítez, N., Sanchez, S. F., et al. 2006, The Astronomical Journal, 132, 926
- Condon, J. J., Cotton, W. D., Greisen, E. W., et al. 1998, The Astronomical Journal, 115, 1693
- Dahlen, T., Mobasher, B., Faber, S. M., et al. 2013, The Astrophysical Journal, 775, 93
- de Vaucouleurs, G. 1948, Annales d'Astrophysique, 11, 247
- Ficarra, A., Grueff, G., & Tomassetti, G. 1985, Astronomy and Astrophysics Supplement Series, 59, 255
- Flewelling, H. A., Magnier, E. A., Chambers, K. C., et al. 2016, eprint arXiv:1612.05243, arXiv:1612.05243
- Gaia Collaboration, G., Brown, A. G. A., Vallenari, A., et al. 2016a, Astronomy & Astrophysics, Volume 595, id.A2, 23 pp., 595, arXiv:1609.04172
- Gaia Collaboration, G., Prusti, T., de Bruijne, J. H. J., et al. 2016b, Astronomy & Astrophysics, Volume 595, id.A1, 36 pp., 595, arXiv:1609.04153
- Griffith, M. R., & Wright, A. E. 1993, The Astronomical Journal, 105, 1666
- Hasselfield, M., Hilton, M., Marriage, T. A., et al. 2013, Journal of Cosmology and Astroparticle Physics, 2013, 008
- Høg, E., Fabricius, C., Makarov, V. V., et al. 2000, Astronomy and Astrophysics, 355, L27
- Huchra, J. P., Geller, M. J., Henry, J. P., & Postman, M. 1990, The Astrophysical Journal, 365, 66
- Hunter, J. D. 2007, Computing in Science & Engineering, 9, 90
- Ilbert, O., Capak, P., Salvato, M., et al. 2009, The Astrophysical Journal, 690, 1236
- Jenkins, A., Frenk, C. S., White, S. D. M., et al. 2001, Monthly Notices of the Royal Astronomical Society, 321, 372
- Kirk, B., Hilton, M., Cress, C., et al. 2015, Monthly Notices of the Royal Astronomical Society, 449, 4010
- Komatsu, E., Smith, K. M., Dunkley, J., et al. 2011, The Astrophysical Journal Supplement Series, 192, 18
- Liu, J., Hennig, C., Desai, S., et al. 2015, Monthly Notices of the Royal Astronomical Society, 449, 3370
- Menanteau, F., Hughes, J. P., Jimenez, R., et al. 2009, The Astrophysical Journal, 698, 1221
- Menanteau, F., Hughes, J. P., Barrientos, L. F., et al. 2010a, The Astrophysical Journal Supplement Series, 191, 340
- Menanteau, F., González, J., Juin, J.-B., et al. 2010b, The Astrophysical Journal, 723, 1523
- Menanteau, F., Sifón, C., Barrientos, L. F., et al. 2013, The Astrophysical Journal, 765, 67
- Molino, A., Benítez, N., Ascaso, B., et al. 2017, Monthly Notices of the Royal Astronomical Society, 470, 95
- Mommert, M., & M. 2017, Astronomy and Computing, 18, 47
- Ochsenbein, F., Bauer, P., & Marcout, J. 2000, Astronomy and Astrophysics Supplement Series, 143, 23
- Oke, J. B. 1974, The Astrophysical Journal Supplement Series, 27, 21
- Oppenheimer, B. R., Helfand, D. J., & Gaidos, E. J. 1997, The Astronomical Journal, 113, 2134
- Perez, F., & Granger, B. E. 2007, Computing in Science & Engineering, 9, 21
- Planck Collaboration, Ade, P. A. R., Aghanim, N., et al. 2011, Astronomy & Astrophysics, 536, A1
- . 2014a, Astronomy & Astrophysics, 571, A20
- . 2014b, Astronomy & Astrophysics, 571, A29
- . 2015, Astronomy & Astrophysics, 582, A29
- . 2016a, Astronomy & Astrophysics, 594, A27
- . 2016b, Astronomy & Astrophysics, 586, A139
- Rengelink, R. B., Tang, Y., de Bruyn, A. G., et al. 1997, Astronomy and Astrophysics Supplement Series, 124, 259
- Sifón, C., Battaglia, N., Hasselfield, M., et al. 2016, Monthly Notices of the Royal Astronomical Society, 461, 248
- Streblyanska, A., Barrena, R., Rubino-Martin, J. A., et al. 2018, eprint arXiv:1804.01356, arXiv:1804.01356
- Sunyaev, R. A., & Zeldovich, Y. B. 1972, Comments on Astrophysics and Space Physics, 4
- Swetz, D. S., Ade, P. A. R., Amiri, M., et al. 2011, The Astrophysical Journal Supplement Series, 194, 41
- Tauber, J. A., Mandolesi, N., Puget, J.-L., et al. 2010, Astronomy and Astrophysics, 520, A1
- The Astropy Collaboration, Robitaille, T. P., Tollerud, E. J., et al. 2013, Astronomy & Astrophysics, 558, A33
- Tinker, J., Kravtsov, A. V., Klypin, A., et al. 2008, The Astrophysical Journal, 688, 709
- Tody, D. 1993, Astronomical Data Analysis Software and Systems II, 52
- Valdes, F. G., & Swaters, R. A. 2007, in Astronomical Society of the Pacific Conference Series, Vol. 376, Astronomical Data Analysis Software and Systems XVI, ed. R. Shaw, F. Hill, & D. Bell, 273
- Voges, W., Aschenbach, B., Boller, T., et al. 1999, Astronomy and Astrophysics, 349, 389
- . 2000, IAU Circulars, 7432
- Wenger, M., Ochsenbein, F., Egret, D., et al. 2000, Astronomy and Astrophysics Supplement Series, 143, 9
- York, D. G., Adelman, J., Anderson, John E., J., et al. 2000, The Astronomical Journal, 120, 1579
- Zwicky, F., & Kowal, C. T. 1968, “Catalogue of Galaxies and of Clusters of Galaxies”, Volume VI (Pasadena, California: California Institute of Technology)